Journal of Alloys and Compounds 748 (2018) 26–35

Contents lists available at ScienceDirect

Journal of Alloys and Compounds

journal homepage: http://www.elsevier.com/locate/jalcom

TLP repaired IN738LC superalloy with uneven surface defect gap width after post heat treatment: Microstructure and mechanical properties

Y. Ye [a, b], G. Zou [a], W. Long [b], H. Bai [a], A. Wu [a], L. Liu [a, *], Y. Zhou [a, c]

[a] Department of Mechanical Engineering, State Key Laboratory of Tribology, Tsinghua University, Beijing, China
[b] The State Key Laboratory of Advanced Brazing Filler Metals & Technology, ZRIME, Zhengzhou, China
[c] Department of Mechanical & Mechatronics Engineering, University of Waterloo, Waterloo, Canada

ARTICLE INFO

Article history:
Received 20 December 2017
Received in revised form
5 February 2018
Accepted 28 February 2018
Available online 2 March 2018

Keywords:
IN738LC
Borides
Heat treatment
Shear strength

ABSTRACT

Cracks repairing of superalloy is very important to the aerospace industry. Most of the crack repairing studies have the same "crack width" which is quite different from the taper-shaped crack in reality. In this study tapered slots with maximum 200 μm width were artificially made by femtosecond laser in small plates of IN738LC superalloy to imitate service cracks. The "cracks" were repaired by diffusion brazing with a mixed filler alloy at 1100 °C for 24 h and followed by homogenization at temperatures of 1160 °C (HT-1), 1180 °C (HT-2) and 1190 °C (HT-3). With increasing homogenization temperature and time, the volume faction of borides in diffusion affected zone (DAZ) decreased. During the homogenization with HT-3, most of the borides in the DAZ of the joint dissolved, merely a small quantity of others coarsened by Ostwald ripening. In order of the processes as-bonded, HT-1, HT-2 and HT-3, the chemical composition of the isothermal solidification zones (ISZs) gradually came close to that of the base metal and the hardness of the ISZs increased, while the hardness of the DAZs decreased. A uniform bonded joint could be obtained with HT-3, and the shear strength of the joint reached up to approximately 95% of the base metal. The corresponding fracture path and fractography of the samples were observed to explain the mechanism of strength evolution.

1. Introduction

IN738LC is a nickel-based superalloy strengthened by solid solution and precipitation hardening mechanisms. It is widely used as hot section components of aero-engines and land based power generation turbines, due to its excellent high temperature strength, hot corrosion resistance and oxidation resistance [1,2]. However, exposed in harsh service conditions, the components usually fail due to thermal fatigue, creep and hot corrosion. Owing to the high cost of manufacturing the superalloy components, the repair of the expensive parts are preferred rather than replacement [3–5]. Substantial amount of alloying elements of Al and Ti (Al + Ti > 6 wt %) have been added to In738LC to improve the mechanical properties at high temperature. However, such high content of the elements makes the material very difficult to be welded because of its high susceptibility to solidification cracking within fusion zone and heat affected zone (HAZ) during welding or post-weld heat treatment [6–11]. To overcome the problem, diffusion brazing of the materials under isothermal solidification or so called transient liquid phase (TLP) bonding has been developed. This method combining benefits of liquid phase bonding and solid-state bonding is considered as an ideal technique for repair of In738LC [12,13]. In TLP bonding process, melting point depressants (MPDs), such as boron and silicon, are added to the braze alloy to lower the bonding temperature that is between the liquidus of the filler metal and the solidus of the base metal. An ideal TLP bonding needs sufficient time for completion of isothermal solidification and is free of undesirable defects [14–18].

Post bonding heat treatment (PBHT) is used to chemically homogenize the joint and accordingly improve mechanical properties [19]. For example, Bakhtiari et al. [20] studied the TLP bonding of FSX-414 using a standard solution cycle and then homogenized at a standard aging condition. The homogenized joint showed more uniform distribution of allying elements and higher shear strength

* Corresponding author.
E-mail address: liulei@tsinghua.edu.cn (L. Liu).

https://doi.org/10.1016/j.jallcom.2018.02.343
0925-8388/

in comparison with the unhomogenized joint. But this treatment failed to remove intermetallics within the joint. Abbasi-Khazaei et al. [21] compared the FSX-414/IN-738 joints homogenized at various temperatures of 1175, 1200 and 1225 °C for 6 h, and found that the highest shear strength of the joints can be obtained after homogenized at 1200 °C. Cao et al. [22] studied the bonding of Inconel718 using a Ni-Cr-Si-B interlayer and followed by the post-weld heat treatment. The results showed the precipitates in the middle of the joint formed in post-weld heat treatment were beneficial to the improvement of the mechanical properties of the joint. Shakerin et al. [23] investigated the bonding of IN738LC utilizing AMS 4777 filler alloy. Solution treatment (1120 °C/2 h) was carried out in two different sequences, one before and another after TLP bonding, accompanying subsequent aging treatment (845 °C/24 h), called HT-A and HT-B, respectively. The highest shear strength was obtained at HT-A. However, the microstructure and mechanical properties of the joints after PBHT were yet to be studied.

Most of studies were carried out using the samples with a uniform gap, which is quite different from the taper-shaped crack in reality. Moreover, most of the gaps studied were less than 100 μm, which were smaller than the real cracks. The isothermal solidification time of bonding IN738 with a large gap, eg. >200 μm was much longer than that with a narrow gap, leading to a larger amount of blocky and acicular borides in DAZ. Therefore, in real application, the post heat treatment (eg. time and temperature) of a TLP repaired crack which is strongly related to the bond strength was quiet different and the study was more challenging. In this research, simulated service cracks with maximum 200 μm width fabricated by femtosecond laser were used for the TLP repair. The research was aimed to investigate the microstructural evolution and the mechanical properties of the brazed joints with various homogenization parameters, and thus to obtain a reliable joint.

2. Experimental procedure

The base metal used in the present study was as-cast IN738 superalloy and the filler metal used was a mixed powder of 50 wt% BNi-1a and 50 wt% DF-4B. The chemical compositions are listed in Table 1. The solidus and liquidus of the BNi-1a braze alloy are 975 and 1075 °C, respectively and the solidus and liquidus of the DF-4B 1065 and 1120 °C, respectively. The 2 mm thick base metal was cut into 10 mm × 5 mm pieces by electro-discharge machining (EDM). The samples were ground using 600 grit SiC paper and ultrasonically cleaned in acetone for 30min.

Fig. 1 shows the experimental procedure. The tapered notches, with approximately 200 μm opening width and 1.2 mm depth, were cut by femtosecond laser under argon shielding. The cross sectioned samples showed that the cutting had not brought about damage of the base metal, as observed in our previous work [24]. A mixture of filler alloys was used to repair the gaps by diffusion brazing. To achieve the homogeneous mixture, BNi-1a and DF-4B powders were mixed on a magnetic stirring for 72 h. The filler metal powders were made into pastes by mixing a liquid binder, which can evaporate upon heating. The TLP bonding was conducted in a vacuum furnace under a vacuum of 10^{-4} Torr to 10^{-5} Torr at 1100 °C for 24 h. PBHT was carried out in the vacuum furnace with the processes 1100 °C/18 h + 1160 °C/6 h (HT-1), 1100 °C/18 h + 1160 °C/6 h + 1170 °C/6 h + 1180 °C/12 h (HT-2), 1100 °C/18 h + 1160 °C/6 h + 1170 °C/6 h + 1180 °C/12 h (HT-2) +1190 °C/6 h (HT-3), respectively.

All the samples were cross sectioned by EDM, mechanically polished and then etched in a solution of 10 g CuCl2 + 40 mL HCL +60 mL methanol. Microstructure was observed by optical microscopy (OM), scanning electron microscopy (SEM) and transmission electron microscopy (TEM). Semi-quantitative analysis of the chemical compositions of the joints were conducted by a SEM (Merlin VP Compact) and TEM (TECHAI G220) equipped with X-ray energy dispersive spectrometer (EDS). Quantitative analysis was also carried out using wavelength-dispersive spectroscopy (WDS) on a JEOL JXA-8230 electron probe micro-analyzer (EPMA).

Micro-hardness tests across the joints of all the specimens were carried out under a 25g load on a Buehler micro-hardness tester. Room temperature shear strength tests were conducted on a Gleeble 1500D thermos-mechanical simulator at a loading speed of 1 mm/min. The shear samples were obtained by removing the part of the base metal below the brazed zone. The testing fixture used for determining the shear strength of the joints is schematically shown in Fig. 2.

3. Results and discussion

3.1. Microstructure of the joints

Fig. 3 (a) shows the microstructure of the joint bonded at 1100 °C for 24 h (as-bonded). The joint consisted of two zones marked by red dash lines, namely isothermal solidification zone (ISZ) and diffusion affected zone (DAZ), respectively. The single solid solution phase of the ISZ indicated that complete isothermal solidification had been obtained [25,26]. Fig. 3 (b)-(d) exhibit the microstructure of the joints homogenized with different heat treatment procedures of HT-1, HT-2 and HT-3. As seen in Fig. 3 (b), although the joint underwent homogenization heat treatment HT-1, the microstructure of the joint appeared unchanged in comparison with the joint as bonded. The DAZ still contained a large number of blocky and acicular precipitates. However, with increasing the temperature and time to HT-2, most of the precipitates dissolved and the alloying elements in the DAZ area adjacent to the ISZ diffused away to low concentration region, resulting in widening of the ISZ, as shown in Fig. 3 (c). When the joint was heat treated with HT-3, intensive diffusion of the alloying elements led to a more uniform microstructure with less precipitates in DAZ. As a consequence, the borders between the DAZ and the ISZ almost vanished, as indicated in Fig. 3 (d).

3.1.1. Diffusion affected zone

Fig. 4 (a)-(b) shows the SEM micrographs of DAZ in as-bonded sample. Large amount of blocky and acicular precipitates

Table 1
Chemical compositions of IN738LC and braze alloys (at%).

Material	Element												
	C	Cr	Co	W	Mo	Fe	Al	Ti	Nb	Ta	Si	B	Ni
IN738LC	0.47	17.33	8.08	0.79	1.14	–	7.27	4.22	0.54	0.55	–	–	Bal.
BNi-1a	0.24	13.12	–	–	–	3.93	–	–	–	–	7.81	13.52	Bal.
DF-4B	–	13.68	12.93	–	–	–	6.59	–	–	0.70	–	12.83	Bal.
Mixed filler alloy	0.12	13.35	6.31	–	–	2	3.22	–	–	0.34	3.97	13.18	Bal.

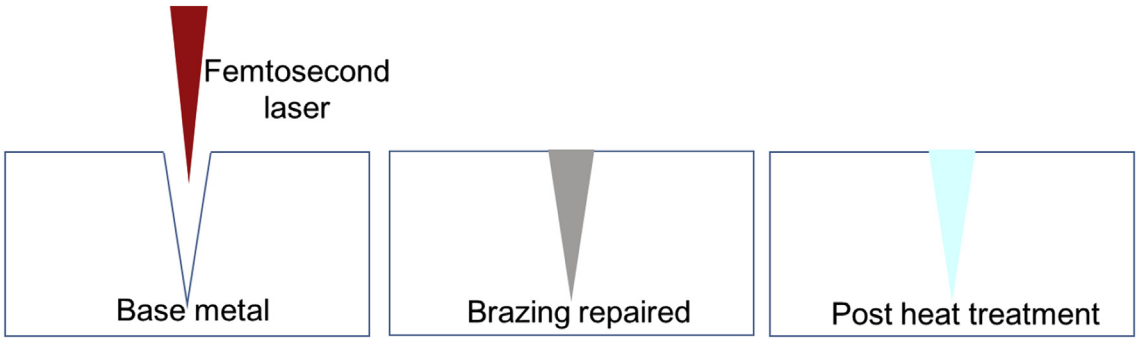

Fig. 1. Schematic diagrams of experimental procedure.

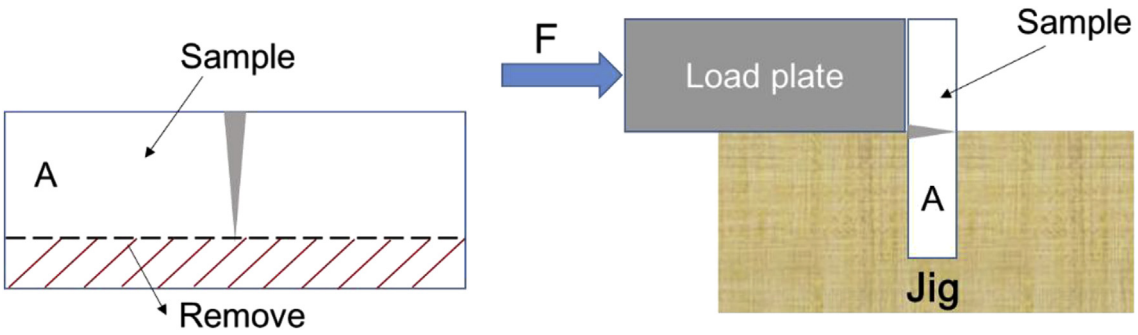

Fig. 2. Schematic diagrams of shear strength testing.

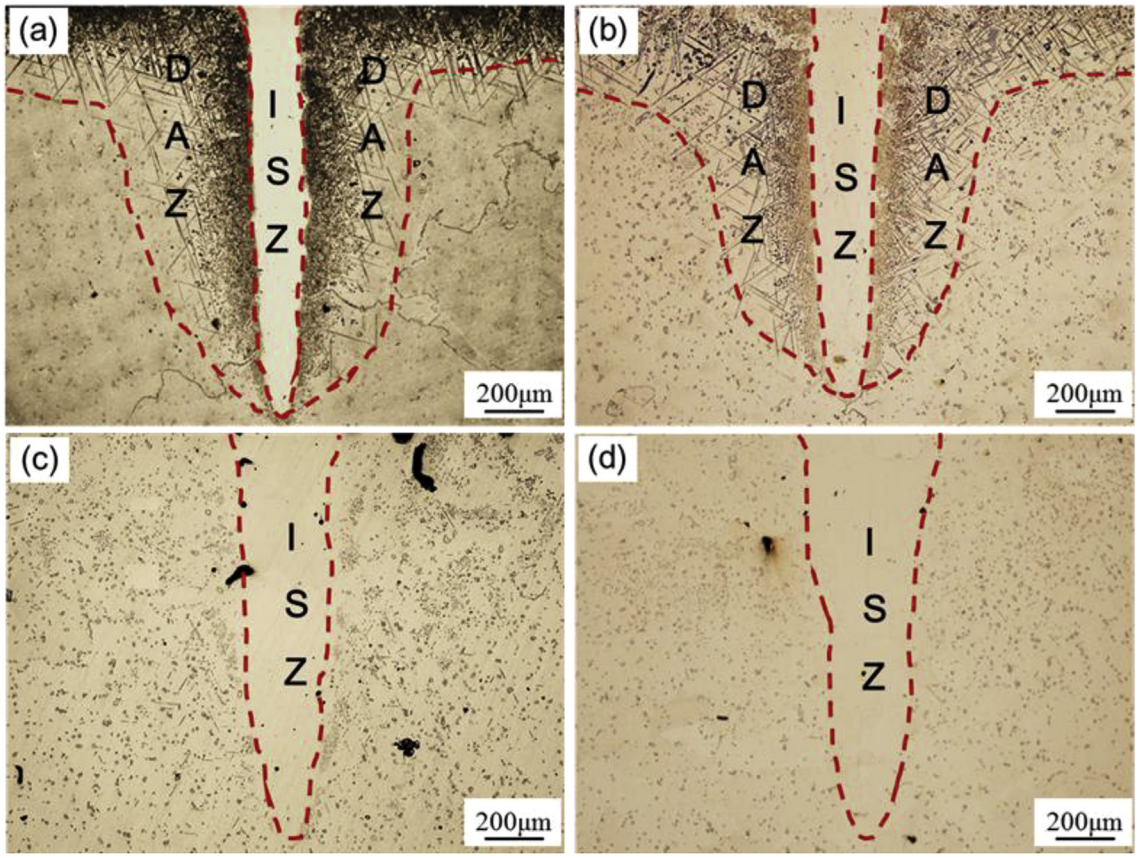

Fig. 3. Optical micrograph of joints: (a) as-bonded, (b) HT-1, (c) HT-2, (d) HT-3.

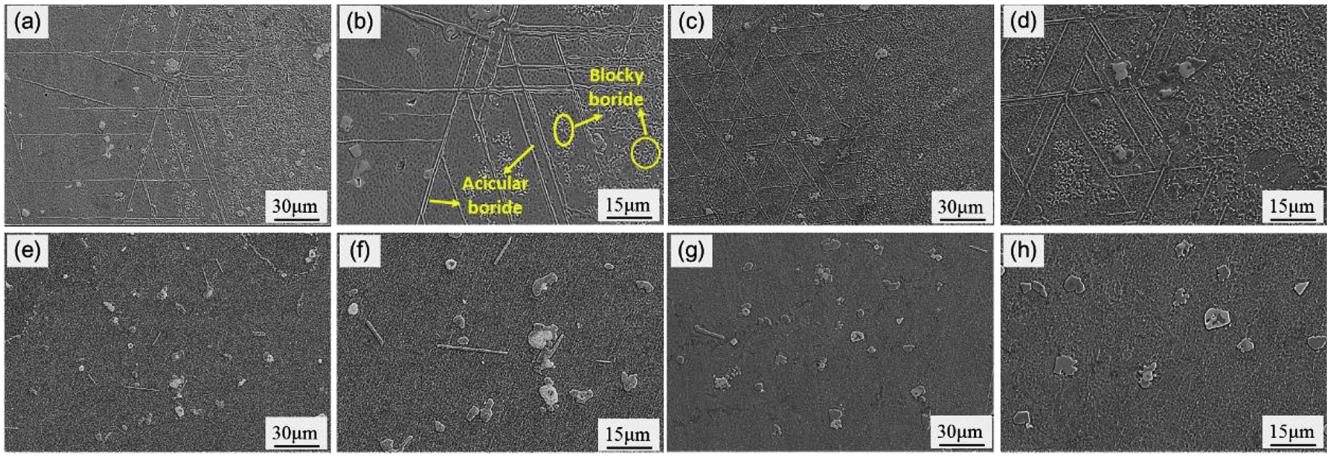

Fig. 4. SEM micrographs of DAZ: (a)–(b) as-bonded, (c)–(d) HT-1, (e)–(f) HT-2, (g)–(h) HT-3.

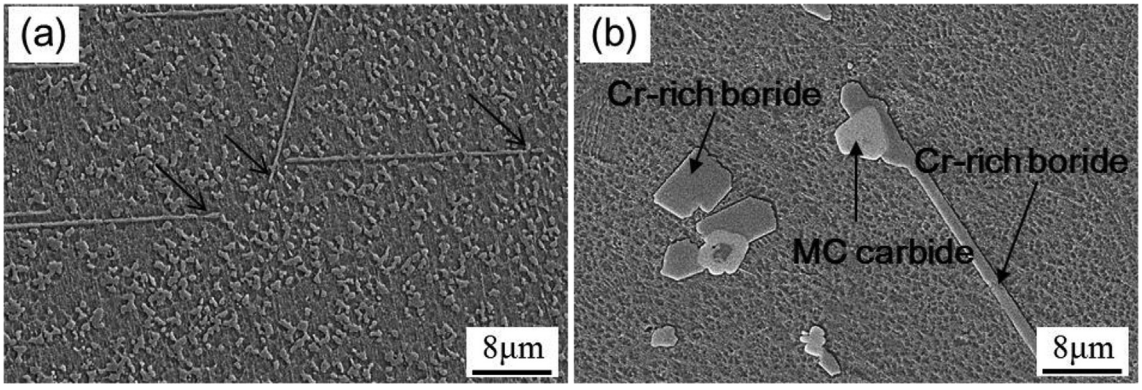

Fig. 5. SEM micrographs of borides in DAZ: (a) as-bonded, (b) HT-3.

presented in the DAZ. Previous study suggested that the precipitates could be Cr-Mo-W rich borides [27]. After heat treated with HT-1, the amount and morphology of the precipitates in DAZ changed little in comparison with the as-bonded sample, as shown in Fig. 4 (c)-(d). Therefore, HT-1 was considered to be insufficient to dissolve the borides in the DAZ. The microstructure of DAZ heat treated with HT-2 is shown in Fig. 4 (e)-(f). Significant decrease in quantity of the precipitates in the DAZ implied that strong diffusion occurred with the heat treatment. It was noted that the undissolved blocky precipitates had progressively coarsened and the length of the acicular precipitates shortened. Fig. 4 (g)-(h) exhibit DAZ of the joint heat treated with HT-3, where the coarsened precipitates scattered. Fig. 5 (a) and (b) show high magnification SEM images of DAZs of the joints as bonded and treated with HT-3. EDS analysis, as listed in Table 2, confirmed that the blocky and acicular precipitates were borides.

The microstructural evolution of the DAZs of the joints, either as bonded or treated with various procedures, was controlled by boron diffusion and equilibrium solubility of the borides at the temperatures. The highest temperature applied to HT-1 was 1160 °C, at which the borides were still undissolved. Since the solubility of the borides and coefficient of the B diffusion contributing to dissolving of the borides exponentially increases with temperature, most of the borides were dissolved with the heat treatment of HT-2 although the highest temperature of HT-2 was 1180 °C, just 20 above 1160 °C. The B separated from the borides diffused into the low concentration area of the base metal in distance. During the homogenization of the brazed joints, the B diffusion obeyed Fick's second law.

Table 2
EDS analysis of borides in DAZ accompanied by TEM (at%).

Element	Cr	Mo	W	B
Blocky boride	6.9	0.8	0.7	91.6
Acicular boride	5.6	1.1	1.0	92.3

The concentration of the B at a distance of x after time t can be expressed as:

$$K\,(C,\,x) = D\,t \tag{1}$$

where K is a parameter decided by C and x, D is diffusion coefficient.

The diffusion coefficient of B in IN738 is given by Arrhenius equation

$$D = D_0 \exp\left(\frac{-Q}{RT}\right) \tag{2}$$

where R is the gas constant, Q is the activation energy for diffusion of B, T is the absolute treating temperature and D_0 is the frequency factor.

Combining equations (1) and (2):

$$K\,(C,\,x) = t\,D_0 exp\left(\frac{-Q}{RT}\right) \tag{3}$$

Q is considered to be invariant at 1150–1190 °C. In this case, the temperature has the most profound influence on the coefficient and diffusion rate because the diffusion coefficient increased in order of magnitude with the increase in temperature. When heat treated with HT-3, the effect of the high temperature on the borides dissolving and the microstructural evolution were significant. As the result, the relatively homogeneous joint was achieved. However, at the temperatures and holding time of HT-3, some undissolved borides coarsened duo to Ostwald ripening, as indicated in Fig. 5 (b).

TEM micrograph of acicular and blocky borides in DAZ is shown in Fig. 6. The chemical compositions of the two borides were comparable. Both of them were composed of Cr, W and Mo and identified as Cr-W-Mo borides (Table 2). The selected area electron diffraction (SAED) patterns of the borides are shown in Fig. 6 and their indexing are listed in Table 3. Both of the borides had the same crystal structure, a hexagonal structure.

Table 3
The indexed results of the SAED.

Radiation radius	Plane distance(Å)		Plane	Angle	
	Practical	Theoretical		Practical	Theoretical
R_{11}	3.9756	3.9800	(006)	68.13	68.29
R_{12}	3.0070	2.9410	(303)		
R_{13}	3.9625	3.9800	(006)	90.31	90.00
R_{14}	2.0802	2.0730	(410)		
R_{15}	5.4856	5.4900	(110)	90.23	90.00
R_{16}	4.0024	3.9800	(006)		
R_{21}	3.9685	3.9800	(006)	69.01	68.29
R_{22}	2.9386	2.9410	(303)		

3.1.2. Isothermal solidification zone

Microstructure of ISZs undergone various heat procedures were observed under SEM. The observations were concentrated on three regions of the ISZ from the top to the bottom, as schematically marked in Fig. 7. As shown in Fig. 7 (a)-(c), the ISZ of as-bonded sample was composed of γ solid solution and tiny cubical γ′ precipitate. When the sample was brought up to the bonding temperature of 1100 °C, the filler melted because B depressed the melting point. The base metal adjacent to the filler liquid dissolved and the liquid increased in volume. This led to the liquid composition to change from original filler to high content of alloying elements, such as Al, Ti, Cr and Co. During holding at the temperature, the B diffused away from the liquid to the base metal and more alloying elements from base metal into the melted zone due to the concentration gradients of the elements. With the decrease in concentration of B, the liquid increased its melting point up to the bonding temperature and then isothermally solidified. Since the ISZ was highly alloyed with Al and Ti, the γ′ precipitated during bonding. It is noted that the ISZ was not chemically homogeneous, as listed in Table 4. The content of Ni, Fe and Si decreased from zone I to zone III, while the content of Cr, Al, Ti and Co showed the opposite distribution. The longer diffusion distance between base metal and the filler metal from zone III to zone I caused the compositional differences, which was explained in our previous study [27]. Although the alloying elements diffused during the bonding, the composition of the ISZ was still nonuniform due to the sluggishness of the diffusion. After heat treated for long time at high temperatures (HT-1, HT-2 and HT-3), which are higher than the solution temperature of γ′, the tiny γ′ disappeared, as shown in Fig. 7 (d)-(l). The chemical compositions of the three zones of the samples with various heat treatment were also detected by EMPA, as summarized in Table 4. The heat treatment with HT-1, HT-2 and HT-3, the temperature and holding time increased in sequence and the diffusion of the alloying elements in the joints was accordingly intensified. As the result, the content of Ni, Fe and Si in the ISZs decreased, while the Cr, Co, Al and Ti increased. Table 4 shows that the chemical composition of the ISZ heat treated with HT-3 gradually came close to that of base metal.

In order to investigate chemical uniformity of the joints, concentrations of Cr, Ni and Al across the joints with different heat conditions, were measured by WDS, as shown in Fig. 8. Ni is the matrix element of the base metal, Al and Cr primarily contributed to the precipitate γ′ and the solid solution, respectively. As can be seen in the figure, the Ni and Al uniformly distributed across the joints with different heat treatments. However, there were a lot of Cr peaks appeared in the DAZs of the joints as bonded and heat treated with HT-1, suggesting that Cr containing precipitate, i.e. the borides densely formed in the zones. Nevertheless, the Cr peaks greatly decreased in the DAZs with post heat treatments of HT-2 and HT-3. Especially, when heat treated with HT-3, the borides in the DAZ significantly dissolved and a homogeneous joint was achieved.

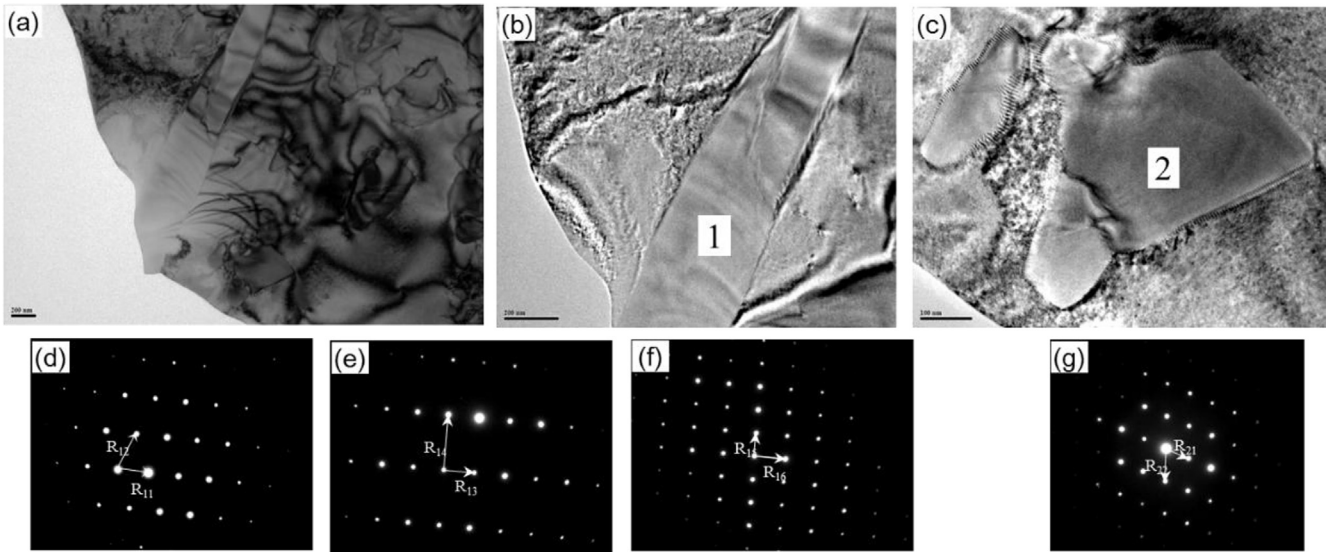

Fig. 6. TEM micrographs of (a) borides: enlarge of (b) acicular boride, (c) blocky boride and the corresponding SAED patterns: (d)–(f) acicular boride, (g) blocky boride.

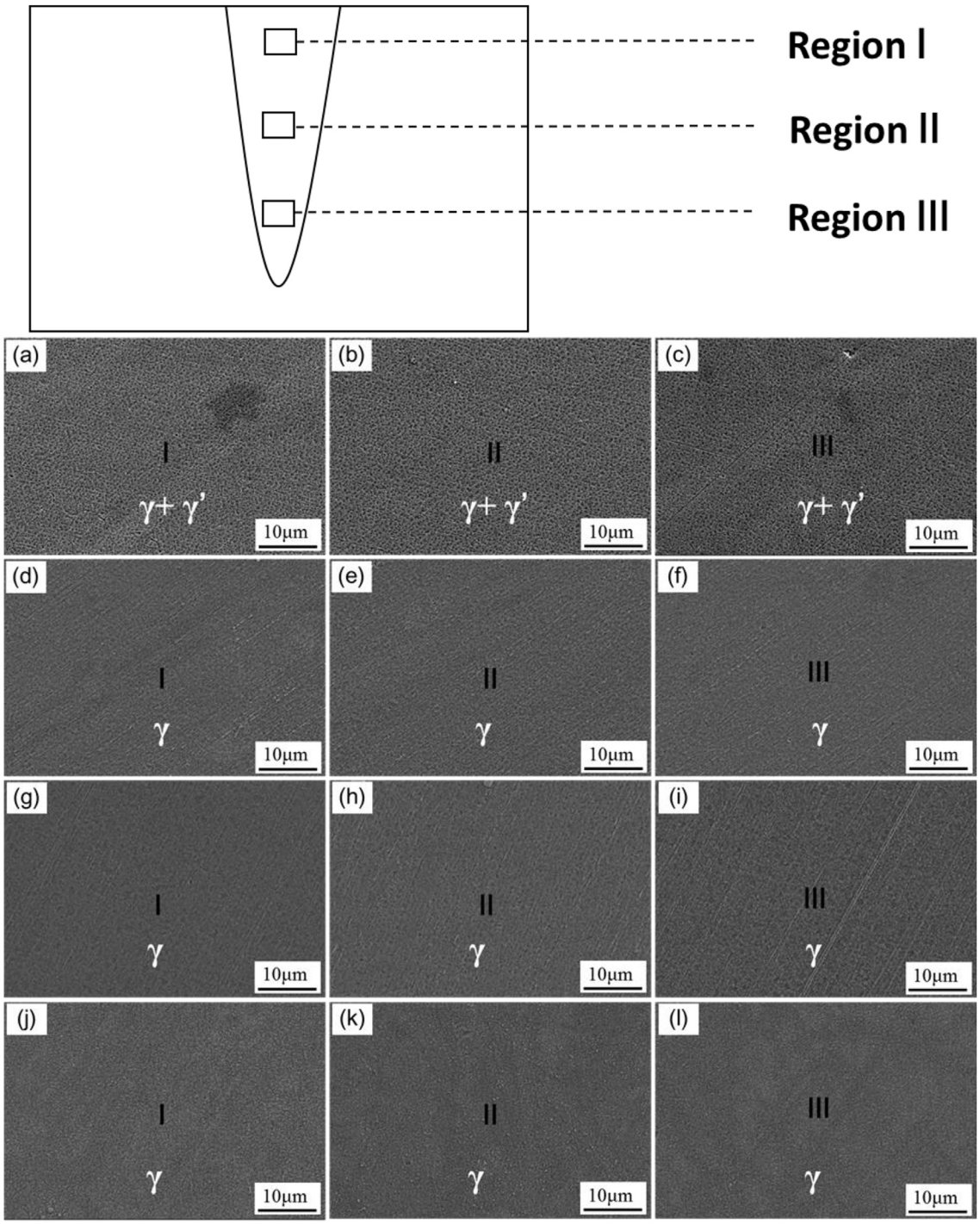

Fig. 7. SEM micrographs of ISZ in different from top to the bottom with different heat conditions: (a)–(c) as-bonded, (d)–(f) HT-1, (g)–(i) HT-2, (j)–(l) HT-3.

3.2. Microhardness

Micro-hardness testing across the joint was used to quantitatively evaluate the mechanical properties and the degree of homogenization of the bonded joints. Fig. 9 shows the hardness values across the joints of the as-bonded, HT-1, HT-2 and HT-3 samples.

The hardness of ISZ increased in order of the joints as-bonded, HT-1, HT-2 and HT-3. This was due to the diffusion of alloying elements, such as Cr, Al, Ti and Co, into the joints. The higher temperature and longer holding time the heat treatment, the more alloying elements diffused from base metal into ISZ, consequently, the ISZs were further solid solution hardened. It is noted that the hardness of DAZs were much higher than that of the BM and ISZs. This was contributed to the precipitates formed in the DAZs. The peak value of the sample as bonded was 650HV, and the average values gradually decreased with the heat treatments with HT-1, HT-2 and HT-3 due to the dissolution precipitates in the DAZ. In the case of HT-3, the hardness of the DAZ decreased to the value comparable to that of the ISZ and base metal. The result further

Table 4
Chemical composition of ISZs from top to the bottom with different heat conditions (at %).

Heat condition		Element						
		Ni	Cr	Al	Ti	Co	Fe	Si
As-bonded	I	67.55	12.33	5.74	0.90	5.71	2.48	5.29
	II	67.80	11.90	6.21	1.16	5.85	2.16	4.91
	III	65.82	13.23	7.02	1.78	6.40	1.81	3.94
	average	**67.06**	**12.49**	**6.32**	**1.28**	**5.99**	**2.15**	**4.71**
HT-1	I	66.26	12.65	6.41	1.91	6.79	2.27	3.72
	II	65.96	13.11	6.73	1.94	6.48	2.20	3.59
	III	63.62	15.10	6.97	2.94	7.86	1.12	2.38
	average	**65.28**	**13.62**	**6.70**	**2.26**	**7.04**	**1.86**	**3.23**
HT-2	I	64.43	14.54	6.83	2.87	6.89	1.98	2.47
	II	63.86	14.63	7.02	3.02	7.29	1.48	2.71
	III	63.31	15.10	7.10	3.14	7.90	1.06	2.39
	average	**63.87**	**14.76**	**6.98**	**3.01**	**7.36**	**1.51**	**2.52**
HT-3	I	63.24	15.41	6.90	3.22	7.27	1.43	2.54
	II	63.07	15.64	7.09	3.50	7.58	0.74	2.37
	III	62.40	16.01	7.17	3.29	7.95	1.09	2.10
	average	**62.90**	**15.69**	**7.05**	**3.34**	**7.60**	**1.09**	**2.34**

corroborated that the uniform joint was achieved by heat treatment with HT-3. It may be seen in Fig. 9 (d), the hardness of the BM unchanged under different conditions, except a little increase near the ISZ due to a small number of precipitates residual in the area.

3.3. Shear strength and fractography

3.3.1. Shear strength

Fig. 10 shows the shear strength of the samples made with different conditions. The shear strength of the base metal was approximately 670 MPa under the same testing condition. The as-bonded joint had the lowest shear strength of 230 MPa, merely 35% of the base metal shear strength. The effect of heat treating on the shear strength was prominent. The shear strength gradually increased with the homogenization heat treatments HT-1, HT-2 and HT-3. When heat treated with HT-3, the highest shear strength of the joint was obtained. The value could reach up to approximately 640 MPa, 95% of the base metal.

3.3.2. Fracture path

Fracture paths of the sheared samples were observed by OM and

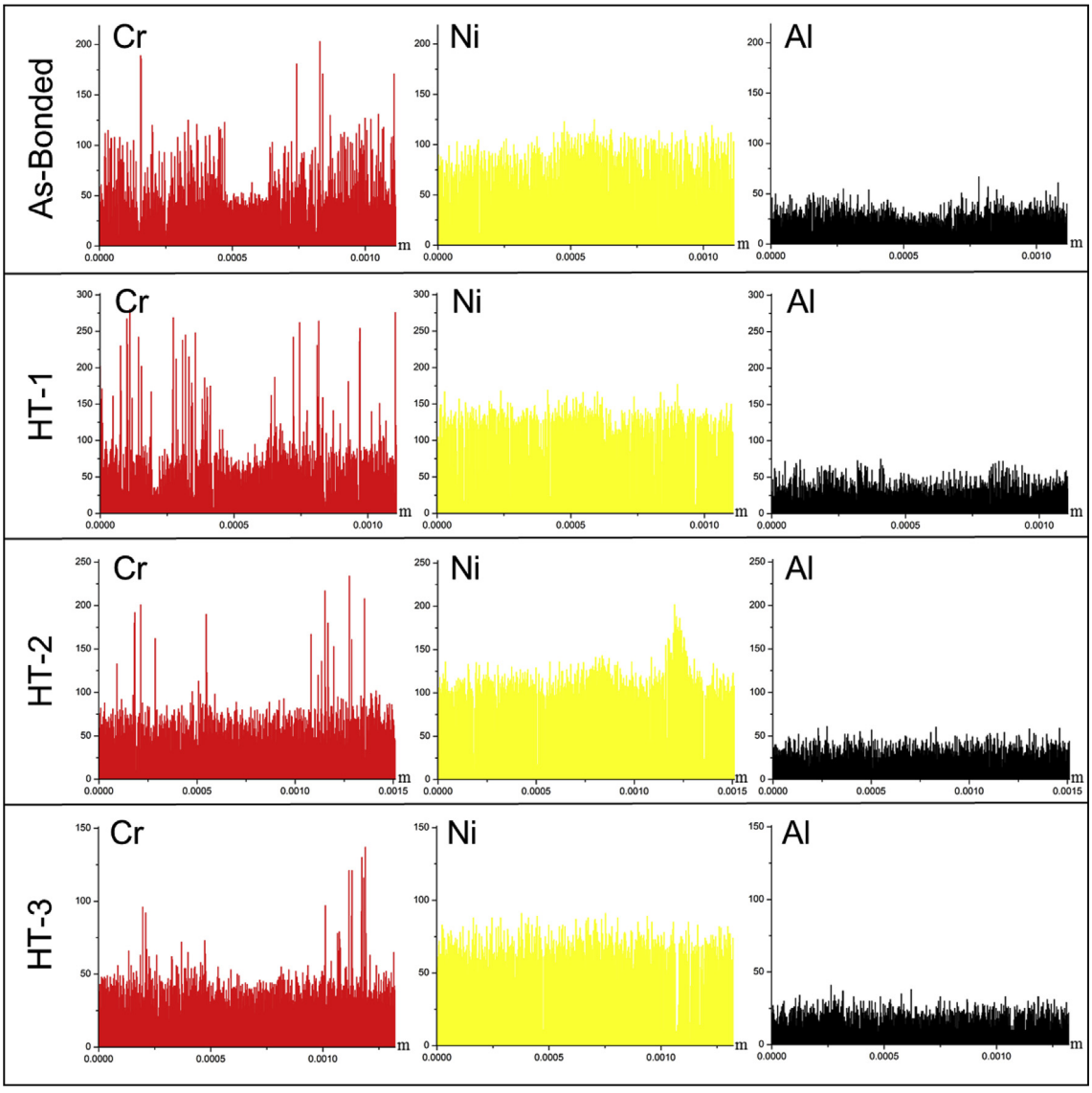

Fig. 8. Line scan across the joints in the case of as-bonded, HT-1, HT-2 and HT-3.

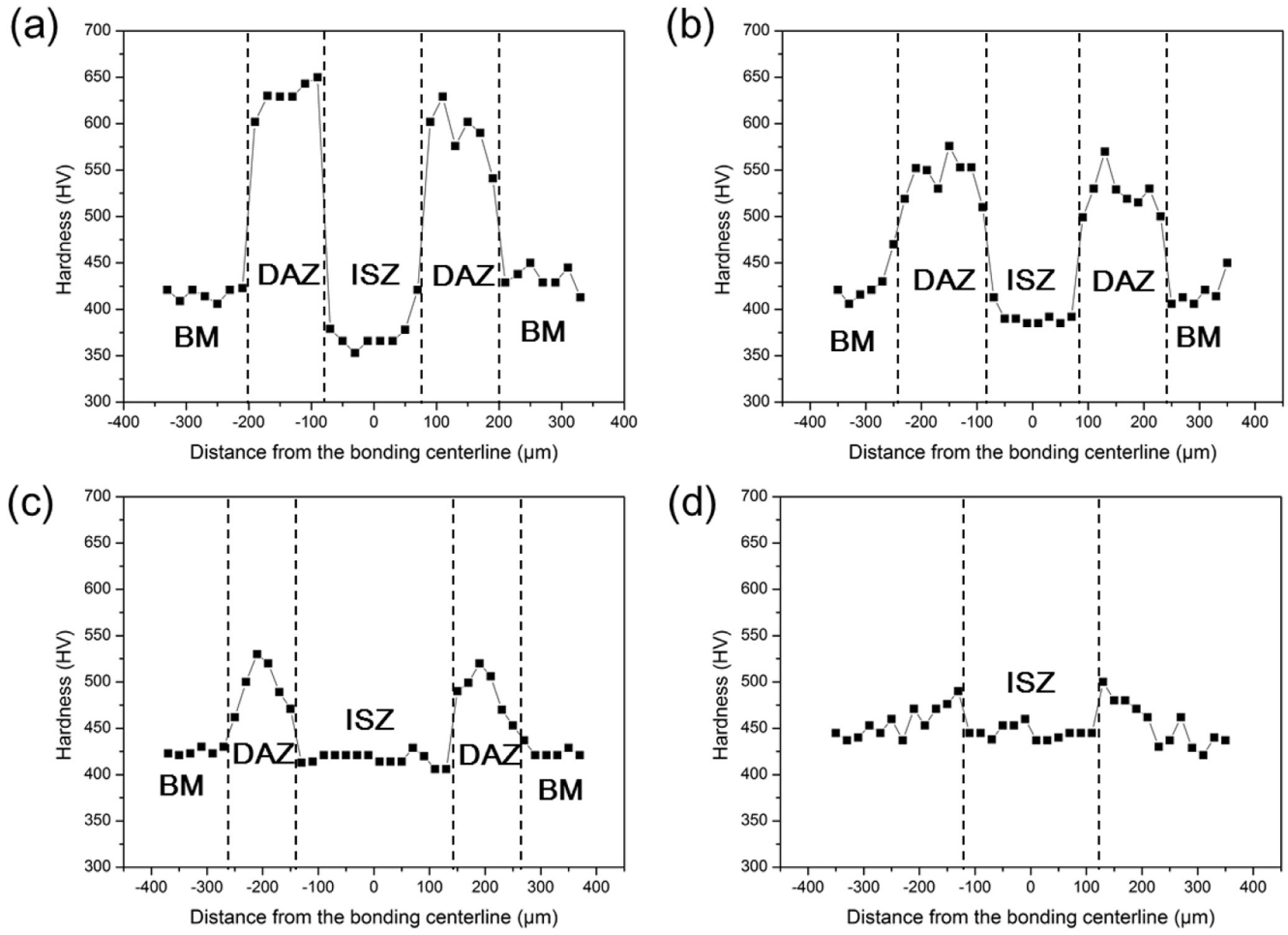

Fig. 9. Hardness values across the joints: (a) as-bonded, (b) HT-1, (c) HT-2 and (d) HT-3 samples.

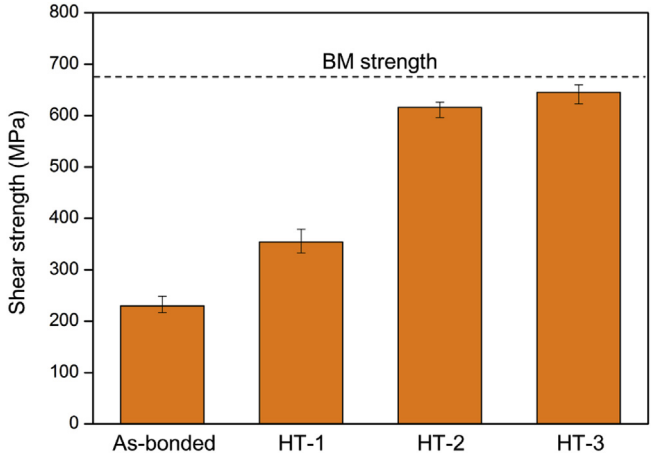

Fig. 10. Comparison of shear strength for joints at different conditions.

SEM, as shown in Fig. 11. Fig. 11 (a) and (e) show the as-bond sample fractured along the acicular borides in DAZ. The dense borides in the DAZ interconnected with each other, offering a continue path of the crack propagation at low stress. Therefore, the joint presented brittle fracture mode and the low shear strength. The fracture path of the joint with HT-1 was situated in DAZ, similar to the sample as-bonded, as shown in Fig. 11 (b) and (f). However, the shear strength of the HT-1 sample increased by ~52%, compared with that of as-bonded sample (shown in Fig. 10). The reason will be explained in the following paragraph. In the case of the sample with HT-2 shown in Fig. 11 (c), the fracture also propagated through DAZ, yet plastic deformation was obviously observed and the fracture path gradually turned close to the ISZ (middle of the joint). The detail of the path was observed using SEM (shown in Fig. 11 (g)), the fracture occurred along tiny blocky borides and substrate in the DAZ. It is believed the decrease of precipitates in the DAZ led to the fracture feature. The resultant shear strength of HT-2 sample increased by 74%, compared with that of HT-1. The HT-3 sample showed a mixed fracture path, partially in ISZ and partially in DAZ, shown in Fig. 11 (d) and (h). It was due to the further decrease in borides in the DAZ.

3.3.3. *Fractography*

Fig. 12 shows the fracture morphologies of the samples as-bonded, HT-1, HT-2 and HT-3 heat treated. The fracture surface of the as-bonded sample (shown in Fig. 12 (a)) presents stepped morphology characterized by cleavage and the steps corresponded to the acicular borides in DAZ. It is believed that the continual borides provided a site of the crack initiation and a path in favor of and propagation, resulting in the low shear strength of the sample [28]. After homogenized with HT-1 (shown in Fig. 12 (b)), the fracture morphology of the joint shows a similar feature to that of as-bonded sample but the cleavage facets are smaller. Tearing cracks are observed on the riser of the steps due to discontinuity of

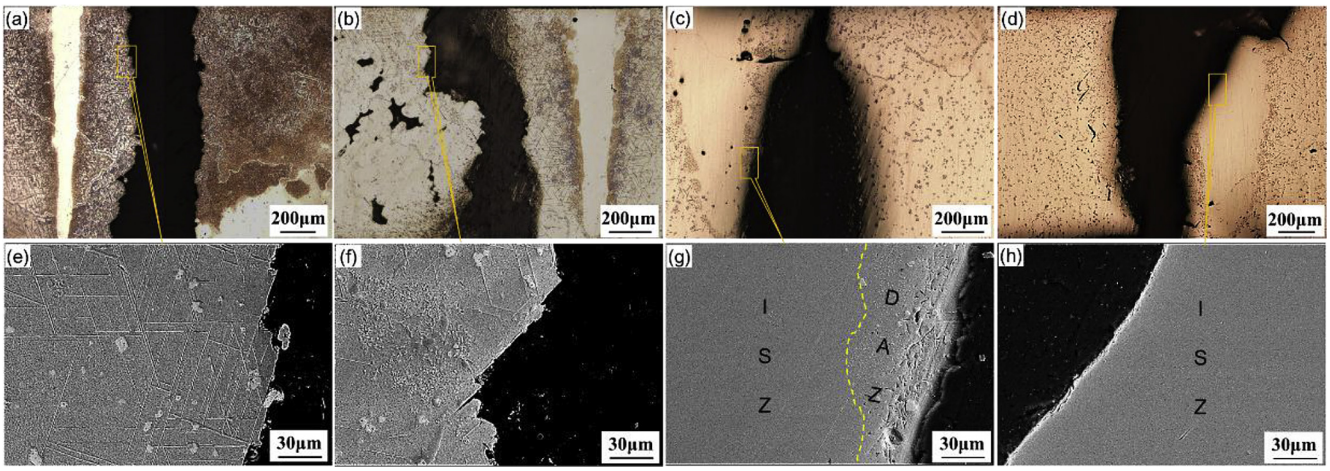

Fig. 11. Fracture paths of (a)–(e) as-bonded, (b)–(f) HT-1, (c)–(g) HT-2, (d)–(h) HT-3.

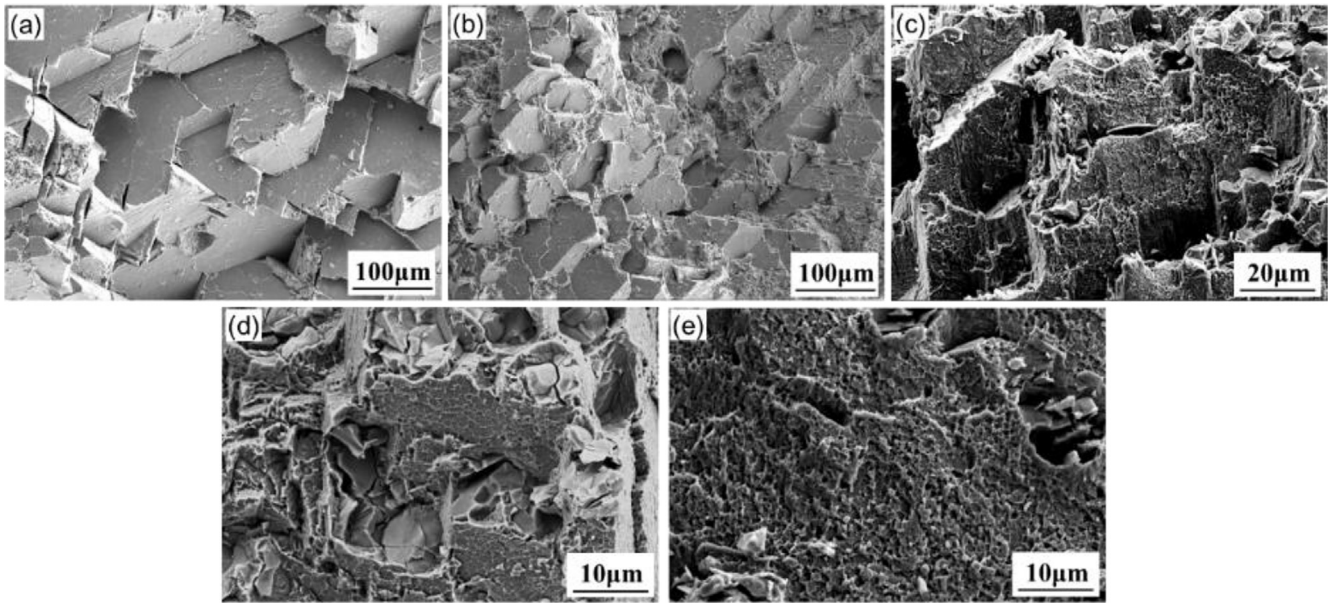

Fig. 12. Fracture morphologies of: (a) as-bonded, (b) HT-1, (c) HT-2 and (d)–(e) HT-3.

borides at the areas. The fracture surface the HT-2 sample in Fig. 12 (c) shows a stepped morphology featured by dimples and cleavage, corresponding to base metal and borides in the DAZ. The sample fractured in a mixed ductile-brittle mode. The fracture surface of HT-3 sample shows two types of morphologies because the crack propagated across ISZ and DAZ. Interspersed shallow dimples and split particles presented on the DAZ (Fig. 12 (d)). Dimples predominated on the fracture surface of the ISZ (Fig. 12 (e)). The feature of the fracture confirmed that the joint with HT-3 indicated as least moderately ductile. Accordingly, the joint exhibited high shear strength in comparison with others.

4. Conclusions

Laser-cut cracks with about 200 μm maximum width in IN738LC superalloy were diffusion brazed and then homogenized under different conditions. The main conclusions are drawn as follows:

1. The diffusion brazed joint presented chemical and microstructural inhomogeneity. Aided by heat treatment, the joint can be chemically homogenized and the precipitates formed in the joint can be dissolved.
2. In order of the joints as-bonded, HT-1, HT-2 and HT-3, the chemical composition of the ISZs gradually came close to that of base metal due to the inter-diffusion of elements between joint and the base metal. The chemical composition across the joint were uniformed after the HT-3 treatment.
3. The hardness of ISZs increased in order of the joints as-bonded, HT-1, HT-2 and HT-3, while that of DAZs decreased. A uniform hardness across the joint could be obtained with HT-3.
4. The shear strength of the as-bonded joint was approximately 35% of the base metal. After homogenized in order of HT-1, HT-2 and HT-3, the shear strength gradually increased and the highest shear strength of the joint, approximately 95% of the base metal, was achieved when heat treated with HT-3. The HT-3 sample presented a mixed fracture mode after shear tested, giving the highest shear strength.

Acknowledgements

This work was supported by National Natural Science Foundation of China (Grant No. 51520105007, 51775299), National Key Research and Development Program of China (2017YFB1104900).

References

[1] C.G. Bieber, Suffern, J.J. Galka, U.S. Patent 3,459,545, 1969.
[2] L. Xiao, D.L. Chen, M.C. Chaturvedi, Cyclic deformation mechanisms of precipitation-hardened Inconel 718 superalloy, Mater. Sci. Eng. A 483 (2008) 369–372.
[3] D. Nagy, X. Huang, Wide gap braze repair using vertically laminated repair scheme, J. Eng. Gas Turbines Power 131 (2009) 012101.
[4] A. Hu, D. Bridges, S. Zhang, Z. Feng, Nanobrazing for turbine blade and vane repair, Adv. Mater. Process. 175 (2017) 25–29.
[5] D. Bridges, C. Ma, Z. Palmer, S. Wang, Z. Feng, A. Hu, Laser brazing of Inconel® 718 using Ag and Cu-Ag nanopastes as brazing materials, J. Mater. Process. Technol. 249 (2017) 313–324.
[6] J.M. Vitek, The effect of welding conditions on stray grain formation in single crystal welds-theoretical analysis, Acta Mater. 53 (2005) 53–67.
[7] C. Tan, W. He, X. Gong, L. Li, J. Feng, Influence of laser power on microstructure and mechanical properties of fiber laser-tungsten inert gas hybrid welded Mg/Cu dissimilar joints, Mater. Des. 78 (2015) 51–62.
[8] A.T. Egbewande, R.A. Buckson, O.A. Ojo, Analysis of laser beam weldability of Inconel 738 superalloy, Mater. Char. 61 (2010) 569–574.
[9] Y. Danis, C. Arvieu, E. Lacoste, T. Larrouy, J.M. Quenisset, An investigation on thermal, metallurgical and mechanical states in weld cracking of Inconel 738LC superalloy, Mater. Des. 31 (2010) 402–416.
[10] L. Li, C. Tan, Y. Chen, W. Guo, F. Song, Comparative study on microstructure and mechanical properties of laser welded–brazed Mg/mild steel and Mg/stainless steel joints, Mater. Des. 43 (2013) 59–65.
[11] M. Montazeri, F.M. Ghaini, The liquation cracking behavior of IN738LC superalloy during low power Nd: YAG pulsed laser welding, Mater. Char. 67 (2012) 65–73.
[12] W.F. Gale, D.A. Butts, Transient liquid phase bonding, Sci. Technol. Weld. Join. 9 (2004) 283–300.
[13] W.D. MacDonald, T.W. Eagar, Transient liquid phase bonding processes, Met. Sci. Join (1992) 93–100.
[14] A. Ghoneim, O.A. Ojo, Microstructure and mechanical response of transient liquid phase joint in Haynes 282 superalloy, Mater. Char. 62 (2011) 1–7.
[15] M. Pouranvari, A. Ekrami, A.H. Kokabi, Microstructure development during transient liquid phase bonding of GTD-111 nickel-based superalloy, J. Alloys Compd. 461 (2008) 641–647.
[16] M. Pouranvari, A. Ekrami, A.H. Kokabi, Effect of bonding temperature on microstructure development during TLP bonding of a nickel base superalloy, J. Alloys Compd. 469 (2009) 270–275.
[17] N.P. Wikstrom, O.A. Ojo, M.C. Chaturvedi, Influence of process parameters on microstructure of transient liquid phase bonded Inconel 738LC superalloy with Amdry DF-3 interlayer, Mater. Sci. Eng. A 417 (2006) 299–306.
[18] V. Jalilvand, H. Omidvar, M.R. Rahimipour, H.R. Shakeri, Investigation on microstructural properties of transient liquid phase (TLP) bonded IN-738LC superalloy with AMS 4776 filler metal, Mater. Sci. Technol. 29 (2013) 439–445.
[19] A. Macwan, X.Q. Jiang, C. Li, D.L. Chen, Effect of annealing on interface microstructures and tensile properties of rolled Al/Mg/Al tri-layer clad sheets, Mater. Sci. Eng. A 587 (2013) 344–351.
[20] R. Bakhtiari, A. Ekrami, Transient liquid phase bonding of FSX-414 superalloy at the standard heat treatment condition, Mater. Char. 66 (2012) 38–45.
[21] B. Abbasi-Khazaei, A. Jahanbakhsh, R. Bakhtiari, TLP bonding of dissimilar FSX-414/IN-738 system with MBF-80 interlayer: the effect of homogenizing treatment on microstructure and mechanical properties, Mater. Sci. Eng. A 651 (2016) 93–101.
[22] J. Cao, Y.F. Wang, X.G. Song, C. Li, J.C. Feng, Effects of post-weld heat treatment on microstructure and mechanical properties of TLP bonded Inconel718 superalloy, Mater. Sci. Eng. A 590 (2014) 1–6.
[23] S. Shakerin, H. Omidvar, S.E. Mirsalehi, The effect of substrate's heat treatment on microstructural and mechanical evolution of transient liquid phase bonded IN-738 LC, Mater. Des. 89 (2016) 611–619.
[24] J. Wei, Y. Ye, G. Zou, Z. Sun, Control of the kerf size and microstructure in Inconel 738 superalloy by femtosecond laser beam cutting, Appl. Surf. Sci. 370 (2016) 364–372.
[25] M. Pouranvari, A. Ekrami, A.H. Kokabi, Solidification and solid state phenomena during TLP bonding of IN718 superalloy using Ni–Si–B ternary filler alloy, J. Alloys Compd. 563 (2013) 143–149.
[26] M. Abdelfatah, O.A. Ojo, Formation of eutectic-type microconstituent during transient liquid phase bonding of nickel: influence of process parameters, Mater. Sci. Technol. 25 (2009) 61–67.
[27] Y. Ye, J. Wei, G. Zou, W. Long, H. Bai, A. Wu, L. Liu, Microstructure of diffusion-brazing repaired IN738LC superalloy with uneven surface defect gap width, Sci. Technol. Weld. Join. 22 (2017) 1–10.
[28] J. Wei, Y. Ye, Z. Sun, G. Zou, H. Bai, A. Wu, L. Liu, The effects of borides on the mechanical properties of TLPB repaired Inconel 738 superalloy, Metall. Mater. Trans. 48 (2017) 4622–4631.